

p-C₆H₄-C₂₀ 的电子结构和紫外光谱

陈 新

(皖西学院 材料与化学学院, 六安 237012)

摘 要: 在 M062X/6-311G(d, p) 水平上优化了 p-C₆H₄-C₂₀ 的基态结构, 计算了该化合物的三种键级 (Mayer、Laplacian 和 Wiberg)、电子空穴分布、定域化轨道指示函数 (LOL) 和红外光谱. 基于 TD-DFT M062X/6-311G(d, p) 方法, 计算了 p-C₆H₄-C₂₀ 在气相中的前 20 个激发态和紫外光谱. π 电子离域分析结果证明, π 电子的离域更可能发生在较短的 C-C 键上, 而不是较长的 C-C, 以及环平面内/外, 而不是环平面上/下. p-C₆H₄-C₂₀ 的两个紫外吸收峰分别位于约 319 nm 和 236 nm 处.

关键词: p-C₆H₄-C₂₀; 键级; 紫外光谱; 电子空穴分析; π 电子离域分析

中图分类号: O56

文献标志码: A

DOI: 10.19855/j.1000-0364.2025.031004

Electronic structure and ultraviolet spectra of p-C₆H₄-C₂₀

CHEN Xin

(School of Materials and Chemical Engineering, West Anhui University, Lu'an 237012, China)

Abstract: Geometry optimization of p-C₆H₄-connected cyclo[20]carbon (p-C₆H₄-C₂₀) was carried out at M062X/6-311G(d, p) level, three kinds of bond orders (Mayer, Laplacian, and Wiberg), electron-hole distributions, localized orbital locators (LOL), and infrared (IR) spectrum were also performed at the same level. Based on TD-DFT M062X/6-311G(d, p) method, the first 20 excited states and ultraviolet (UV) spectra of p-C₆H₄-C₂₀ were calculated. Calculation results of π -electron delocalization analyses prove that π -electron delocalization of p-C₆H₄-C₂₀ is more likely to occur on shorter C-C bonds rather than longer C-C bonds, and inside/outside of the ring plane rather than above/below the ring plane. Two absorption peaks of p-C₆H₄-C₂₀ locate at about 319 nm and 236 nm, respectively.

Key words: p-C₆H₄-C₂₀; Bond orders; UV spectrum; Electron-hole analyses; π -electron delocalization analyses

1 Introduction

Since gas-phase formation of cyclo[18]carbon (C₁₈) was reported by Diederich in 1989^[1], it has been a research hotspot. Its cyclic condensed-phase structure was first observed in 2019^[2]. Until now, large amounts of experimental and computational studies on cyclo[18]carbon were carried out. Li@C₁₈ complex was testified as optical molecular switch under proper external electric field (EEF)^[3]. Coplanar

and perpendicular configurations of C₁₈-graphene nanoribbon junction were current ON and OFF states, respectively, with ON/OFF ratio 10.4^[4]. Diverse transport behaviors of C₁₈-ring connected electrodes molecular devices included Ohmic characteristic, quasi Schottky feature, and current-limiting function, and so on^[5]. C₁₈ also exhibited unique mechanical properties^[6]. To expand application scopes of C₁₈ analogs, p-C₆H₄-C₂₀ was investigated in this work, this structure can be regarded as five C-C tri-

收稿日期: 2023-07-26

基金项目: 安徽省高等学校科研基金(2022AH051686); 皖西学院高层次人才项目(WGKQ2022099)

作者简介: 陈新, 男, 博士, 副教授, 主要从事计算化学研究等. E-mail: cx810101@163.com

ple bonds ($C \equiv C$) of cyclo[20] carbon (C_{20} , in which ten $C \equiv C$ are connected by $C - C$ singlet bonds) were substituted by five phenyl rings evenly.

2 Computational methods

Structural optimization at B3LYP^[7]/6-31G (d), B3LYP/6-311G (d, p), and M062X^[8,9]/6-311G (d, p)^[10] three levels, and ultraviolet spectrum calculation at time-dependent (TD) - M062X/6-311G (d, p) level were carried out using Gaussian 09 program^[11]. M062X method has been proved to be a reliable method for structural optimization and reaction mechanisms of organic systems, especially for those containing weak interactions^[12-17]. Electron density analysis, ultraviolet spectrum drawing, electron-hole analysis^[18], contributions ratio calculation of molecular orbitals (MO) transitions for excited states, and localized orbital locator (LOL) calculation were performed with Multiwfn software^[19].

3 Results and discussion

3.1 Geometric structure

Top view (left) and side view of optimized structure of $p-C_6H_4-C_{20}$ is shown as Fig. 1. As seen in Fig. 1, $p-C_6H_4-C_{20}$ appears to be approximately circular, but it isn't a regular circle actually. Lengths of long axis and short axis of three calculation methods (B3LYP/6-31G*, B3LYP/6-311G**, and M062X/6-311G**) are successively 11.0185 Å and 11.0156 Å, 10.9912 Å and 10.9887 Å, 10.9753 Å and 10.8803 Å, respectively. It can be concluded that rings' structures obtained from the two latter methods shrink slightly compared with that of B3LYP/6-31G*. Furthermore, ring structure of M062X/6-311G** shrinks more pronounced.

C-C bonds (except for those of phenyl rings) are divided into two categories, namely C-C bonds between two phenyl rings (shorter bonds) and C-C bonds connecting with phenyl rings (longer bonds). Schemes of long bonds and short bonds are depicted in Fig. 2. Labels of carbon atoms on molecular ring can be seen in Fig. 3. Bond lengths of longer bonds and shorter bonds calculated at B3LYP/6-31G*,

B3LYP/6-311G**, and M062X/6-311G** three levels are shown in Table 1. As can be seen from Table 1, bond lengths of longer bonds of three methods are in turn about 1.4239 Å, 1.4209 Å, and 1.4286 Å, respectively. Meanwhile, bond lengths of shorter bonds of three methods are in succession about 1.2214 Å, 1.2147 Å, and 1.2079 Å, respectively. So compared with B3LYP/6-31G*, bond lengths are shortened for both shorter C-C bonds and longer C-C bonds for B3LYP/6-311G** calculation results. But for M062X/6-311G**, bond lengths of shorter C-C bonds are shortened, and those of longer C-C bonds are extended. However, the longer C-C bond lengths and the shorter C-C bond lengths of C_{18} optimized at ω B97XD/def-TZVP level are about 1.343 Å and 1.221 Å, respectively^[20]. In comparison, the longer C-C bond lengths are shorter than those of $p-C_6H_4-C_{20}$. In summary, whether for both $p-C_6H_4-C_{20}$ or C_{18} , the shorter C-C bond lengths are between those of (about 1.325 Å) and $C \equiv C$ (about 1.1980 Å), and are not complete triple bonds.



Fig. 1 Top view (left) and side view of optimized structure of $p-C_6H_4-C_{20}$ (H atoms in side view structure are omitted for clarity)

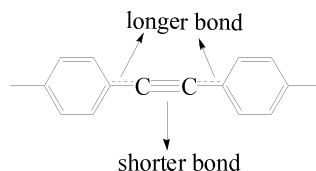


Fig. 2 Schemes of long bonds and short bonds

Three types of bond orders, namely Mayer bond orders, Laplacian bond orders^[21], and Wiberg bond orders were calculated, calculation results are listed in Table 2. Longer C-C bond orders of three methods are about 2.68, 2.37, and 2.66, respectively. While shorter C-C bond orders of three methods are about 1.16, 1.21, and 1.14, respectively. This proves

Table 1 Calculation results of bond lengths using three different methods

Bonds	Lengths(Å)			Bonds	Lengths(Å)		
	A ^a	B ^b	C ^c		A ^a	B ^b	C ^c
C1 – C2	1. 22140	1. 21465	1. 20787	C4 – C21	1. 42388	1. 42092	1. 42860
C3 – C4	1. 22140	1. 21466	1. 20789	C5 – C31	1. 42384	1. 42091	1. 42867
C5 – C6	1. 22141	1. 21466	1. 20787	C6 – C44	1. 42389	1. 42090	1. 42860
C7 – C8	1. 22140	1. 21465	1. 20790	C7 – C53	1. 42384	1. 42093	1. 42859
C49 – C50	1. 22140	1. 21465	1. 20789	C8 – C24	1. 42390	1. 42088	1. 42865
C1 – C34	1. 42388	1. 42092	1. 42860	C49 – C41	1. 42387	1. 42090	1. 42862
C2 – C14	1. 42388	1. 42091	1. 42863	C50 – C56	1. 42387	1. 42091	1. 42861
C3 – C11	1. 42386	1. 42091	1. 42864				

Note: a, b and c are calculation results of B3LYP/6 – 31G^{*}, B3LYP/6 – 311G^{**}, and M062X/6 – 311G^{**}, respectively.

Table 2 Bond orders of C – C bonds in p – C₆H₄ – C₂₀

Bonds	Bond Orders			Bonds	Bond Orders		
	Mayer	Laplacian	Wiberg		Mayer	Laplacian	Wiberg
C1 – C2	2. 67543	2. 37137	2. 65901	C4 – C21	1. 16290	1. 21503	1. 14306
C3 – C4	2. 67517	2. 37363	2. 65902	C5 – C31	1. 16258	1. 21379	1. 14303
C5 – C6	2. 67550	2. 37288	2. 65894	C6 – C44	1. 16249	1. 21519	1. 14310
C7 – C8	2. 67501	2. 37134	2. 65892	C7 – C53	1. 16270	1. 21635	1. 14312
C49 – C50	2. 67609	2. 37114	2. 65898	C8 – C24	1. 16286	1. 21432	1. 14306
C1 – C34	1. 16239	1. 21623	1. 14305	C41 – C49	1. 16261	1. 21636	1. 14307
C2 – C14	1. 16274	1. 21699	1. 14303	C50 – C56	1. 16256	1. 21564	1. 14308
C3 – C11	1. 16293	1. 21435	1. 14303				

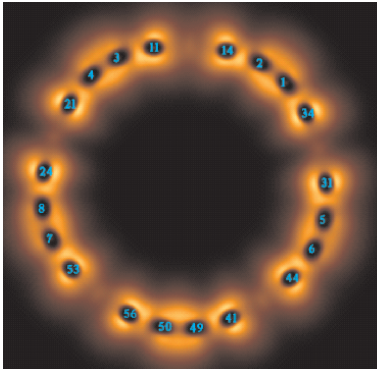


Fig. 3 Color – filled map of localized orbital locator (LOL) – π along the ring plane

that C – C bonds of p – C₆H₄ – C₂₀ ring are not identical, and shorter C – C bonds are not fully triplet bonds.

3.2 Electron density distribution and electron delocalization

Map of electron density at 1 Å above the molecular plane of p – C₆H₄ – C₂₀ can be seen in Fig. 4. In Fig. 4, the brighter the sites, the larger the electron

density. Judged from Fig. 4, electron densities of shorter C – C bonds and longer C – C bonds are different, electron densities of shorter C – C bonds are greater than those of longer C – C bonds. It further proves that C – C bonds on ring of p – C₆H₄ – C₂₀ are not identical. In addition, electron densities p – C₆H₄ – C₂₀ are mainly focused on phenyl rings.

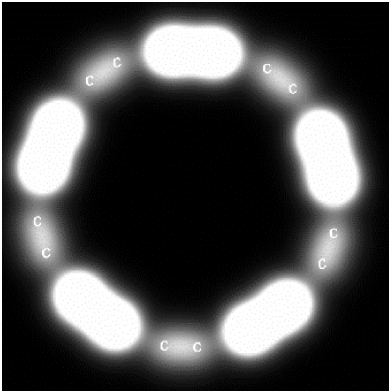


Fig. 4 Map of electron density at 1 Å above the molecular plane of p – C₆H₄ – C₂₀

The π - electronic delocalization situations are shown in Fig. 5. Judged by Fig. 5, π - electronic delocalization above / below the ring plane originates from z - axial π - electron of shorter C - C bonds, while π - electronic delocalization inside/outside (right) the ring plane comes from both phenenyl rings and π - electron of shorter C - C bonds. Meanwhile, there are weak conjugation effect between xy - axial π - electron orbitals of shorter C - C bonds and π - e-lectron orbitals of phenyls. Fig. 3 and Fig. 5 confirm that π - electronic delocalization of p - C₆H₄ - C₂₀ prefers to occur in shorter C - C bonds. Fig. 5 also proves that π - electronic delocalization of p - C₆H₄ - C₂₀ mainly occurs inside / outside (right) of the ring plane. Localizing occupied molecular orbitals containing C1 - C2 bond can be seen in Fig. 6. The left figure of Fig. 6 indicates that C1 - C2 bond bears partial σ charecteristic, the middle and the right figures of Fig. 6 are π - orbitals perpendicular to and parallel to the p - C₆H₄ - C₂₀ ring plane, respectively.

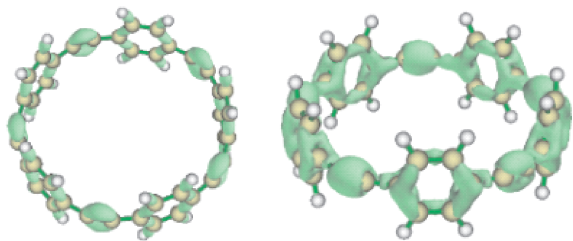


Fig. 5 π - electronic delocalization situations above / below (left) and inside / outside (right) the ring plane

3.3 Ultraviolet spectra

Fig. 7 is UV spectra of p - C₆H₄ - C₂₀. There are two absorption peaks, located at about 319 nm and 236 nm within the region of 200 - 400 nm, respectively. Twenty excited states were calculated, and excited states with larger oscillator strength ($f > 0.1$) are listed in Table 3, corresponding major molecular orbitals (MO) transitions for these excited states are also listed. Because molecular transitions for these excited states are disperse, natural transition orbitals (NTO) analyses (as seen in Table 4) were carried out to define dominant transition contributions. But unfortunately, NTO analyses do not improve transition contributions dramatically.

Energy of HOMO (highest occupied molecular

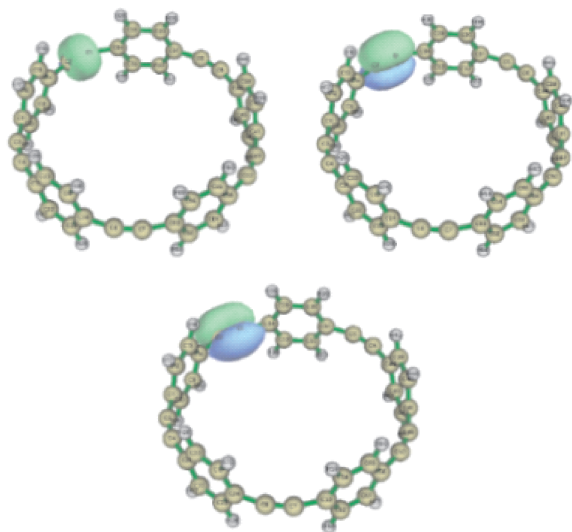


Fig. 6 Localizing occupied molecular orbitals containing C1 - C2 bond

orbitals) and LUMO (lowest unoccupied molecular orbitals) are -6.80528 eV and -1.58846 eV, respectively. HOMO - LUMO gap is 5.21682 eV (503.34638 kJ/mol). Absorption peak at about 319 nm with molar absorption coefficient about 140000 L/mol/cm is very strong, it is mainly due to $\pi \rightarrow \pi^*$ transition of conjugated system, belonging to strong absorption K band. This absorption peak is mainly originated from the contributions of S0 \rightarrow S2 and S0 \rightarrow S3. For S0 \rightarrow S2, contributions of major molecular orbitals transitions come from HOMO \rightarrow LUMO + 1 and HOMO - 1 \rightarrow LUMO, their contributions are 42.1% and 41.9%, respectively. While for S0 \rightarrow S3, contributions of major molecular orbitals transitions come from HOMO \rightarrow LUMO and HOMO - 1 \rightarrow LUMO + 1, and their contributions are both 42.0%.

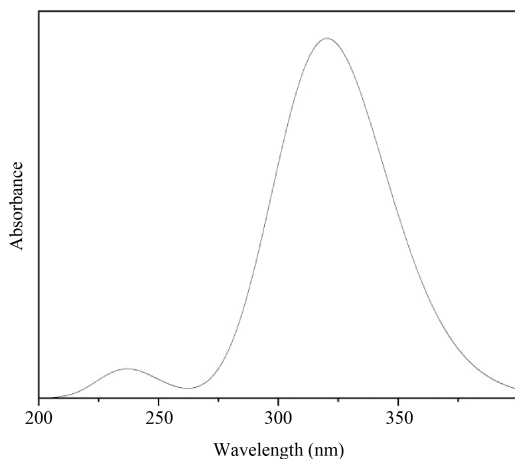


Fig. 7 Ultraviolet spectrum of p - C₆H₄ - C₂₀

Absorption peak at about 236 nm is dramatically weaker than the absorption peak at 319 nm, with about 1/14 intensity of the latter. This absorption peak mainly arises from S0 → S19 and S0 → S20. Contributions of molecular orbitals transitions for S0 → S19

Table 3 Contributions of major molecular orbitals (MO) transitions for various excited states

No.	<i>E</i> (eV)	Wavelength(nm)	<i>f</i>	Major MO transitions
2	3.8841	319.21	1.72450	H→L + 1 42.1% , H - 1→L 41.9%
3	3.8844	319.18	1.72600	H - 1→L + 1 42.0% , H→L 42.0%
19	5.2541	235.98	0.13700	H→L + 2 31.5% , H - 1→L + 3 31.4% , H - 3→L + 1 8.5% , H - 2→L 8.4% , H - 1→L 6.6% , H→L + 1 6.5%
20	5.2542	235.97	0.13710	H→L + 3 31.5% , H - 1→L + 2 31.4% , H - 2→L + 1 8.5% , H - 3→L 8.5% , H - 1→L + 1 6.6% , H→L 6.6%

Note: H and L represent HOMO and LUMO, respectively.

Table 4 Contributions of major natural transition orbitals (NTO) transitions for various excited states

No.	Major NTO transitions
2	NTO 130→NTO 131 48.878% , NTO 129→NTO 132 48.755%
3	NTO 130→NTO 131 48.845% , NTO 129→NTO 132 48.787%
19	NTO 130→NTO 131 40.656% , NTO 129→NTO 132 40.534%
20	NTO 130→NTO 131 40.622% , NTO 129→NTO 132 40.536%

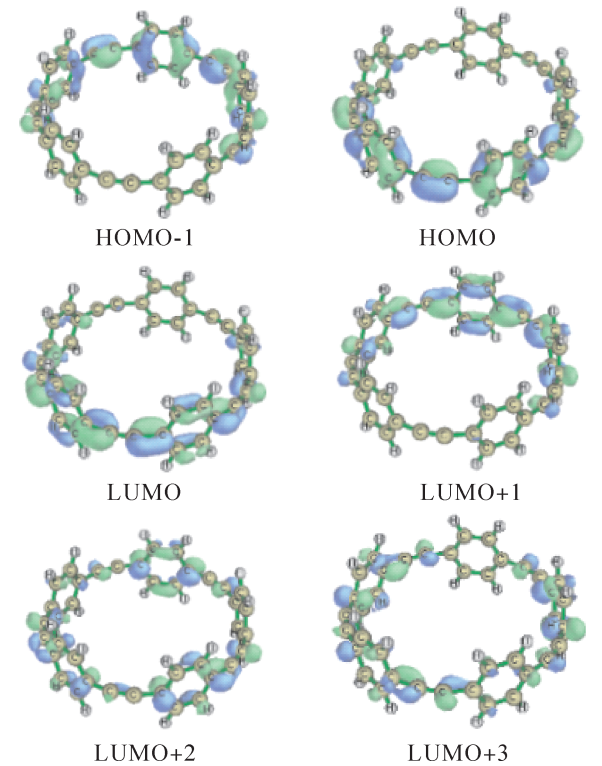


Fig. 8 Schemes of partial frontier molecular orbitals

3.4 Density of states (DOS)

Total and partial density of states (DOS) map of p - C₆H₄ - C₂₀ is shown in Fig. 9. The position of

and S0 → S20 are very dispersed, relative greater contributions originate from transitions of HOMO and HOMO + 1 to LUMO + 2 and LUMO + 3. Judged from Fig. 8, these molecular orbitals transitions can also be ascribed to π→ π* .

dash line at - 6.80528 eV is HOMO. As Fig. 9 shown, the curves were interrupted, occupied orbitals lie on the left of interruption point, while unoccupied orbitals lie on the right of interruption point. In the region of - 21.77 eV ~ 5.44 eV , molecular orbitals are mainly contributed by phenyl rings. Shorter C - C bonds' contributions to molecular orbitals are much smaller, especially in lower - energy region.

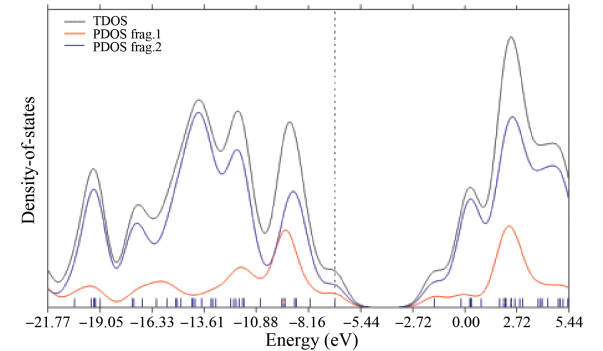


Fig. 9 Total and partial (fragment 1 and 2) density - of - states (DOS) map of p - C₆H₄ - C₂₀ (from top to bottom). (Fragment 1 and 2 are shorter C - C bonds and phenyl rings, respectively)

3.5 Electron - hole analyses

In electron - hole analyses, " hole " and " electron " are the states after electrons are excited. Hence, " hole " and " electron " refer to starting point and arrival point of the excited ground states' electrons, respectively. Calculation values of *D*, *Sr*, *H*, *t*, *E_{coul}*, *Δσ*, *HDI* and *EDI* for transitions from S0 to S2, S3, S19, and S20 are listed in Table 5, and their meanings can be seen in note of Table 5. In

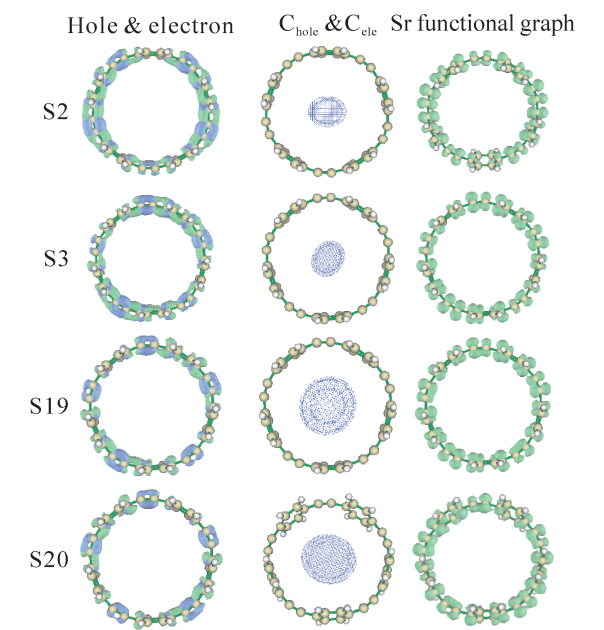
general, the smaller the D value and $\Delta\sigma$ value, the larger the Sr value, the more obvious negative value the t index, the closer the main distribution range of holes and electrons, the more obvious the tendency of local electron excitation. Moreover, the smaller the value of HDI (EDI), the higher the delocalization degree of holes (electrons), that is, the greater the uniformity of distribution and the wider the distribution range. Judged from Table 5, D values of $S0 \rightarrow S2$, $S0 \rightarrow S3$, $S0 \rightarrow S19$, and $S0 \rightarrow S20$ range from 0.002 to 0.005. Compared to $[0 - 1]$ value range of D value, these values are very small. It indicates centroids of hole and electron are almost coincident, this can also be testified by map of Chole & Cele (Fig. 10). Simultaneously, four excitations have sig-

nificant negative t values of ($-3.760 \sim -4.284 \text{ \AA}$), very small $\Delta\sigma$ values ($0.043 \sim 0.057 \text{ \AA}$), relative larger Sr values ($0.85271 \sim 0.89139 \text{ a.u.}$, close to 1), it confirms that separation degree of holes and electrons is very small, and the overlap degree of electrons and holes is very large. This can also be demonstrated by electron – hole distribution map (Hole & electron, Fig. 10). In addition, relative smaller HDI (EDI) values and electron – hole distribution map (Hole & electron, Fig. 10) jointly explain that these four excitations have broader distribution ranges. In summary, $S0 \rightarrow S2$, $S0 \rightarrow S3$, $S0 \rightarrow S19$, and $S0 \rightarrow S20$ bear significant characteristics of local electron excitation (LE excitation).

Table 5 Relevant indexes of the electron – hole distribution

	$D \text{ (\AA)}$	$Sr \text{ (a.u.)}$	$H \text{ (\AA)}$	$t \text{ (\AA)}$	$E_{\text{coul}} \text{ (eV)}$	HDI	EDI	$\Delta\sigma \text{ (\AA)}$
$S0 \rightarrow S2$	0.005	0.85277	5.697	-3.582	3.016913	4.13	3.78	0.044
$S0 \rightarrow S3$	0.002	0.85271	5.695	-4.284	3.017495	4.13	3.78	0.043
$S0 \rightarrow S19$	0.005	0.89045	5.702	-4.172	2.997168	3.91	3.80	0.057
$S0 \rightarrow S20$	0.004	0.89139	5.702	-3.760	2.990704	3.94	3.84	0.057

Note: D , Sr , H , t , E_{coul} , $\Delta\sigma$, HDI and EDI represent index of distance between centroid of hole and centroid of electron, average overlap value of hole and electron, overall average distribution breadth of hole and electron, degree of separation of holes and electrons, hole – electron Coulomb attractive energy, difference of overall spatial distribution between electrons and holes, hole delocalization index and electron delocalization index, respectively.



3.6 IR spectra

Infrared (IR) spectra of $p\text{-C}_6\text{H}_4\text{-C}_{20}$ is shown in Fig. 11. Absorption peaks located at 3214 cm^{-1} and 3198 cm^{-1} are stretching vibration (ν_s) peak of C – H on phenyl rings, and absorption peaks at 1674 cm^{-1} , 1557 cm^{-1} and 1450 cm^{-1} are stretching vibration peaks of benzene rings, while absorption peaks at 2307 cm^{-1} and 1333 cm^{-1} are ν_s of shorter C – C bonds and ν_s of longer C – C bonds, respectively. The strongest peak centered at 863 cm^{-1} is out – of – plane bending vibration peak of C – H on phenyl rings.

4 Conclusions

Based on the optimized geometry of $p\text{-C}_6\text{H}_4\text{-C}_{20}$ molecule, C – C bond lengths were measured and analyzed by Mayer bond orders, Laplacian bond orders, and Wiberg bond orders. The C – C bonds (except for those of phenyl rings) of $p\text{-C}_6\text{H}_4\text{-C}_{20}$ ring

Fig. 10 Hole & electron (left), Chole & cele (middle), and Sr diagram (right)
Note: Hole & electron, Chole & cele, Sr functional graph are hole and electron distribution isosurfaces, centroid isosurfaces of electrons and holes, hole – electron overlap isosurfaces, respectively. In Hole & electron, blue and green isosurfaces represent hole and electron distributions, respectively.

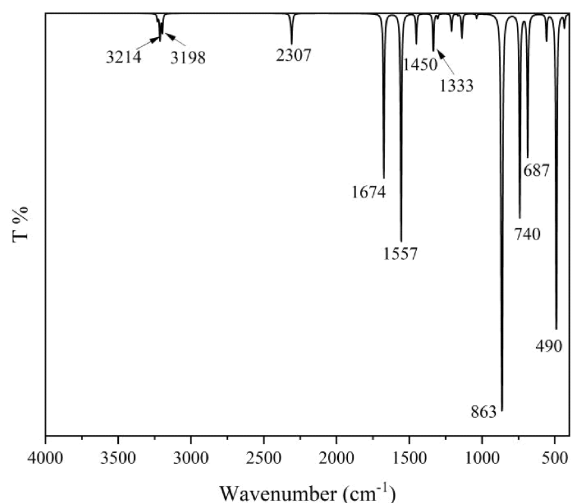


Fig. 11 IR spectrum of p - C₆H₄ - C₂₀

are not equivalent, and the shorter C - C bond lengths are between those of C - C double bond and triple bond. π - electron delocalization analyses results prove that π - electron delocalization of p - C₆H₄ - C₂₀ is more likely to occur on shorter C - C bonds rather than longer C - C bonds, and inside / outside of the ring plane rather than above / below the ring plane. There are two absorption peaks located at about 319 nm and 236 nm, respectively. And the two absorption peaks are mainly contributed by S0→S2, S0→S3, S0→S19, and S0→S20. All these transitions can be attributed to $\pi \rightarrow \pi^*$. Electron - hole analyses results proved these four excitations are all local electron excitation (LE).

References:

[1] Diederich F, Rubin Y, Knobler C B, *et al.* All - carbon molecules: evidence for the generation of cyclo [18]carbon from a stable organic precursor[J]. *Science*, 1989, 245: 1088.

[2] Kaiser K, Scriven L M, Schulz F, *et al.* An sp - hybridized molecular carbon allotrope, cyclo [18] carbon[J]. *Science*, 2019, 365: 1299.

[3] Zeyu L, Xia W, Tian L, *et al.* Potential optical molecular switch: lithium@ cyclo [18] carbon complex transforming between two stable configurations [J]. *Carbon*, 2022, 187: 78.

[4] Yuehua X, Wenjun W. High - efficiency switching effect and negative differential conductance in cyclo [18]carbon - graphene nanoribbon junction[J]. *J. Appl. Phys.*, 2020, 128: 194303.

[5] Zhang L, Li H, Feng Y P, *et al.* Diverse transport be-

haviors in cyclo [18] carbon - based molecular devices[J]. *J. Phys. Chem. Lett.*, 2020, 11: 2611.

[6] Fang S, Hu Y H. Cyclo[18]carbon as an ultra - elastic molecular O - ring with unique mechanical properties[J]. *Carbon*, 2021, 171: 96.

[7] Stephens P J, Devlin F J, Chabalowski C F, *et al.* *Ab initio* calculation of vibrational absorption and circular dichroism spectra using density functional force fields[J]. *J. Phys. Chem.*, 1994, 98: 11623.

[8] Becke A D. Density - functional thermochemistry V. Systematic optimization of exchange - correlation functionals[J]. *J. Chem. Phys.*, 1997, 107: 8554.

[9] Wang Y, Verma P, Jin X, *et al.* Revised M06 density functional for main - group and transition - metal chemistry[J]. *Proc. Natl. Acad. Sci. USA*, 2018, 115: 10257.

[10] Zhao Y, Truhlar D G. The M06 suite of density functionals for main group thermochemistry, thermochemical kinetics, noncovalent interactions, excited states, and transition elements: two new functionals and systematic testing of four M06 - class functionals and 12 other functionals[J]. *Theor. Chem. Acc.*, 2008, 120: 215.

[11] Frisch M J, Trucks G W, Schlegel H B, *et al.* Gaussian 09, Rev. A. 02. Wallingford CT: Gaussian, Inc., 2009.

[12] Chen G H, Jiang N, Xiang H Y, *et al.* Theoretical analysis of structural characteristics of morin rearrangement for cephalosporins prepared from penicillin sulfoxide[J]. *Chinese J. Struct. Chem.*, 2020, 39: 1594.

[13] Cheng X L, Li L Q, Han Y F, *et al.* DFT investigation on the enantioselectivity of olefin carboacylation catalyzed by a Rh (I) complex [J]. *Chinese J. Struct. Chem.*, 2020, 39: 630.

[14] Martin W, Andrew J A H, Ananya S, *et al.* Performance of M06, M06 - 2X, and M06 - HF density functionals for conformationally flexible anionic clusters: M06 functionals perform better than B3LYP for a model system with dispersion and ionic hydrogen - bonding interactions [J]. *J. Phys. Chem. A*, 2013, 117: 12590.

[15] Vyacheslav S B, Mamadou S D, Adri C T D, *et al.* Evaluation of B3LYP, X3LYP, and M06 - Class density functionals for predicting the binding energies of neutral, protonated, and deprotonated water clusters[J]. *J. Chem. Theory Comput.*, 2009, 5: 1016.

[16] Singh I, El - Emam A A, Pathak S K, *et al.* Experimental and theoretical DFT (B3LYP, X3LYP, CAM -

- B3LYP and M06 - 2X) study on electronic structure, spectral features, hydrogen bonding and solvent effects of 4 - methylthiadiazole - 5 - carboxylic acid [J]. *Mol. Simul.*, 2019, 45: 1029.
- [17] Roohi H, Moghadam B. Decomposition mechanism of the phenylaminy C₆H₅NH radical to propargyl and acetylene: a M06 - 2X, CBS - QB3 and G4 study [J]. *Chem. Phys. Lett.*, 2019, 730: 332.
- [18] Liu Z, Lu T, Chen Q. An sp - hybridized all - carbon atomic ring, cyclo [18] carbon: electronic structure, electronic spectrum, and optical nonlinearity [J]. *Carbon*, 2020, 165: 461.
- [19] Lu T, Chen F W. Multiwfn: a multifunctional wavefunction analyzer [J]. *J. Comput. Chem.*, 2012, 33: 580.
- [20] Shi B, Yuan L, Tang T Y, *et al.* Study on electronic structure and excitation characteristics of cyclo [18] carbon [J]. *Chem. Phys. Lett.*, 2020, 741: 136975.
- [21] Lu T, Chen F W. Bond order analysis based on the Laplacian of electron density in fuzzy overlap space [J]. *J. Phys. Chem. A*, 2013, 117: 3100.